ENPH 479 Assignment #5: Finite-Difference Time-Domain

Matt Wright[1,*]

[1] *Department of Physics, Engineering Physics and Astronomy, Queen's University, Kingston, ON K7L 3N6, Canada*

(Dated: April 6, 2022)

The Finite-Difference Time Domain (FDTD) algorithm is a numerical technique to solve Maxwell's equations in some discretized region. We investigated both 1-dimensional and 2-dimensional variations of the algorithm.Beginning with the 1-dimensional case, we implemented absorbing boundary conditions that reflected a wave with about 0.015% of the incident amplitude. Then, we used the total-field scattered-field approach to inject the pulse only in the forward direction. This yielded a backwards wave with an amplitude about 0.001% the size of the forward wave. This was then applied to inject a wave into a dielectric film where we observed a lossless transition and an expected change in frequency in the dielectric. We then investigated more interesting dispersion models, namely the Drude and Lorentz dispersion models. These models specify a frequency dependent dielectric constant that result in lossy media. In all cases, the numerical and analytical solutions agreed almost perfectly. Finally, we shifted our focus to the 2-dimensional formulation of FDTD. We experimented with a uniform region as well as a region with a dielectric slab. Due to the larger computational demand of the problem, we investigated different algorithmic methods of solving the problem. We first optimized the approach by implementing NumPy slicing and nested `for` loop algorithms as well as leveraging Numba or not. This gave 4 different methods to test. It was found that Numba without slicing was the fastest approach for the problem. We then parallelized this optimal approach and tested on regions of 1008 and 3008 cells squared. We noticed a significant improvement for the latter case, decreasing run time from 68.02 s on a single task to 9.91 s on 8 tasks but began to see diminishing return after 8 processes.

I. 1-DIMENSIONAL FDTD

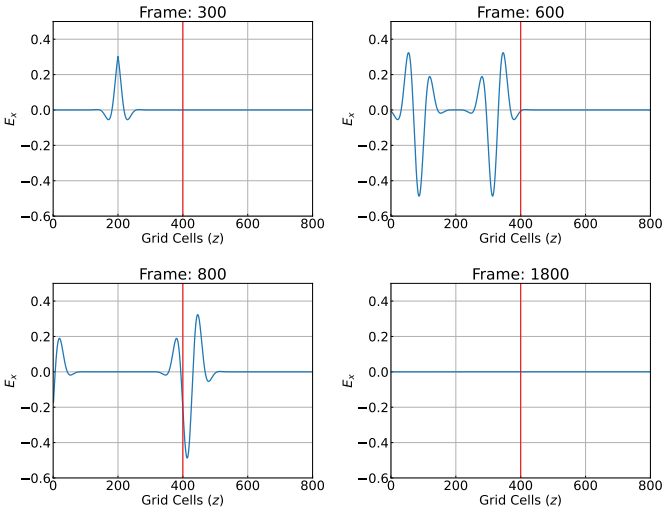

Figure 1. 1-dimensional FDTD simulation of a 2-fs pulse travelling in free space with absorbing boundary conditions. The reflection of these absorbing boundary conditions is given in Fig. 2.

We begin with a simple 1-dimensional simulation of FDTD. First we implement absorbing boundary conditions (ABCs), given by,

$$E_x^n(0) = E_x^{n-2}(1), \tag{1}$$

$$E_x^n(k_{end}-1) = E_x^{n-2}(k_{end}-2). \tag{2}$$

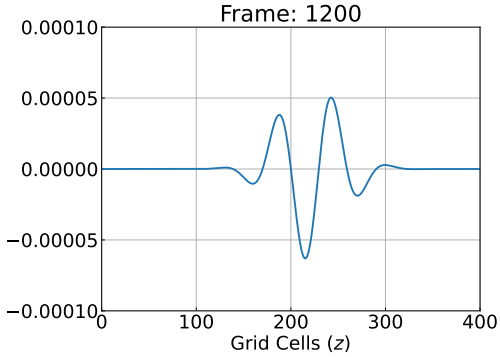

Figure 2. Reflection from the absorbing boundary condition shown in Fig. 1. The maximum amplitude of E_x for the incident pulse is 0.325 units while the reflected wave has a maximum amplitude on the order of 5×10^{-5}.

Snap shots of the injected pulse's evolution are given in Fig. 1. It can be seen here that there is a negligible reflection so we zoom in on the on the reflection in Fig. 2 where we can see the amplitude of the reflected pulse is on the order of 5×10^{-5} units. This is indeed negligible when compared to the initial amplitude which can be seen to be four to five orders of magnitude larger.

Next, we implement the total-field scattered-field approach to inject the pulse only in the forward direction. We do not show snap shots of the pulse (as it is similar to Fig. 1 without the left travelling portion) but instead show the amount that is travelling backwards in Fig. 3. It can be seen that the amplitude traveling backwards is on the order of 1×10^{-5} units. The forward pulse amplitude is on the order of 1 units, which is five orders of magnitude larger.

Finally, we simulate a dielectric film of thickness $L = 1$

* matt.wright@queensu.ca

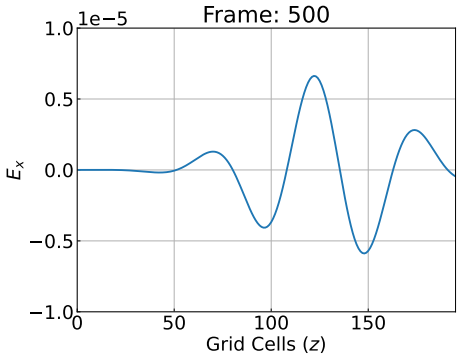

Figure 3. Portion of wave injected backwards from the total-field scattered-field approach. The wave injected forward has an E_x amplitude on the order of 1 while the backwards wave shown has an amplitude near 1×10^{-5}.

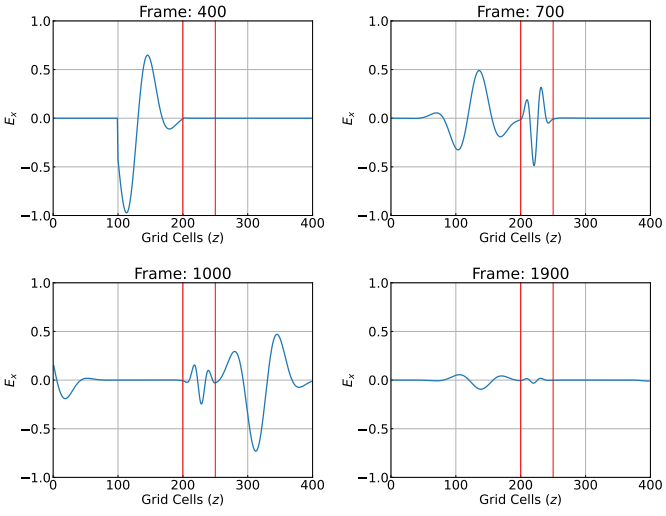

Figure 4. Shapshots of a 1-dimensional FDTD simulation with a 1 micron dielectric with constant $\epsilon = 9$.

micron with dielectric constant, $\epsilon = 9$. Snapshots of injecting a pulse into this system are given in Fig. 4. As expected, the wavelength of the EM wave inside the dielectric decreases and we observe reflections off the dielectric. We also can see that a small amount of the wave is trapped in the dielectric and slowly dissipates. We summarize the electric field in three different sections: the incident, transmitted, and reflected portions. We show portions of the functions in the time-domain and frequency domain in the top and bottom subplots of Fig. 5, respectively. We indeed see the amplitude dissipate with time as it is absorbed by the boundary condition but because of the portion trapped in the dielectric, the dissipation is slower then in free space. We can also see in the bottom of Fig. 5 that the sum of the reflection and transmission coefficients is equal to 1 over the displayed frequency, confirming that this is a lossless system. We can also see that the analytical solutions for the transmission and reflection coefficients[1] agree nicely with

[1] Assuming a harmonic solution of the form $E = E(\omega)e^{-i\omega t}$.

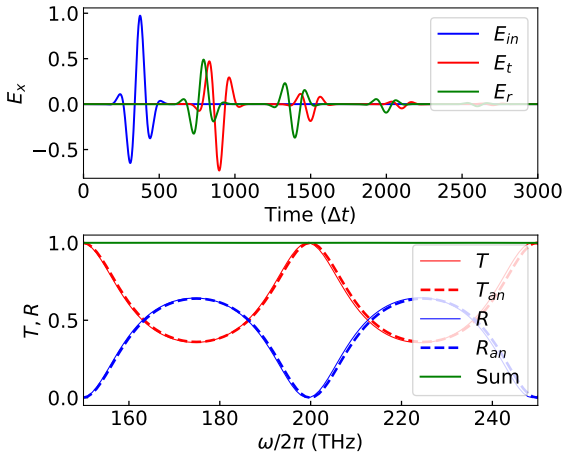

Figure 5. Transmission (T) and reflection (R) coefficients of E_x in the frequency domain for the 1-dimensional FDTD simulation with dielectric film shown in Fig 4. The analytical solutions as well the the sum of T and R are shown.

our numerical results.

II. FLUX DENSITY FDTD AND FREQUENCY-DEPENDENT MEDIA

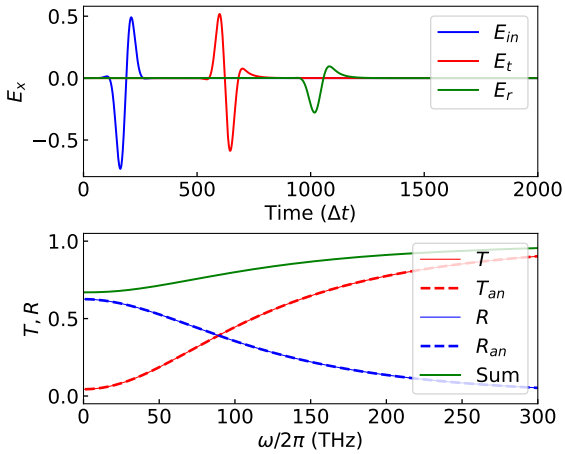

Figure 6. FDTD simulaiton of dielectric film of 200 nm with dielectric constant defined by the Drude dispersion model (Eq. (3)). We show the injected field (E_{in}), transmitted field (E_r), and the reflected field (E_r), as well as their corresponding transmission and reflection coefficients. The simulated and analytical solutions agree almost exactly.

In this section we use the flux density formulation of the Maxwell FDTD solver. The process is effectively the same but now we keep track of vectors for D and E. This formulation allows us to investigate more interesting dielectric materials.

We analyze first the Drude dispersion model with the frequency-depenent dielectric constant give by,

$$\epsilon_D(\omega) = 1 - \frac{\omega_p^2}{\omega^2 + i\omega\alpha}, \tag{3}$$

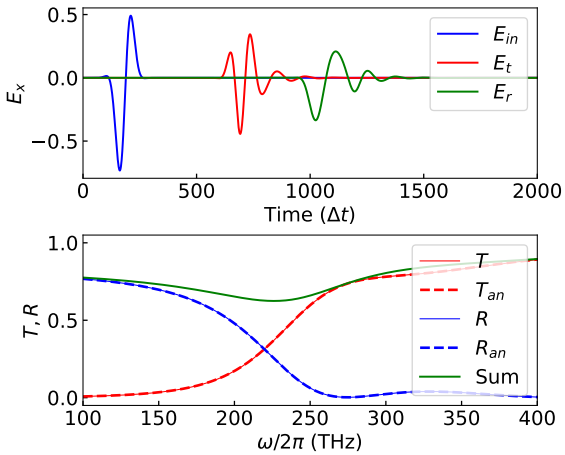

Figure 7. FDTD simulaiton of dielectric film of 800 nm with dielectric constant defined by the Drude dispersion model (Eq. (3)). We show the injected field (E_{in}), transmitted field (E_r), and the reflected field (E_r), as well as their corresponding transmission and reflection coefficients. The simulated and analytical solutions agree almost exactly.

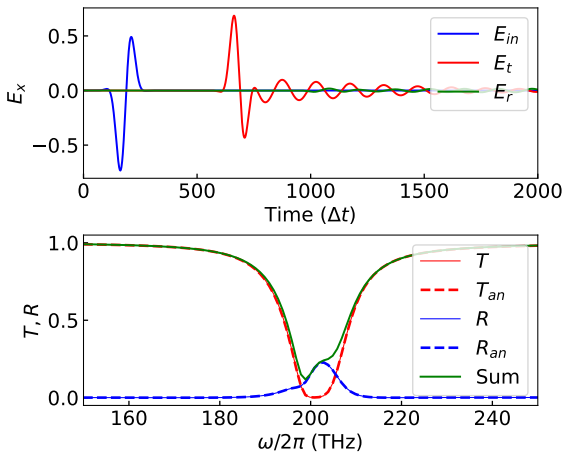

Figure 9. FDTD simulaiton of dielectric film of 800 nm with dielectric constant defined by the Lorentz dispersion model (Eq. (4)). We show the injected field (E_{in}), transmitted field (E_r), and the reflected field (E_r), as well as their corresponding transmission and reflection coefficients. The simulated and analytical solutions agree almost exactly.

where $\alpha = 1.4 \times 10^{14}$ rad/s and $\omega_p = 1.26 \times 10^{15}$ rad/s. We use a 200-THz source, 1-fs Gaussian pulse, and spatial step size of 20 nm. The summarizing plots of of this model for dielectric films of thickness $L = 200$ nm and $L = 800$ nm are shown in Fig. 6 and Fig. 7, respectively. Both plots show that the sum of the transmission and reflection coefficients are no longer equal to 1, which signifies that materials following this dispersion model are lossly. We can also see that there is only one cross-over point between the transmission and reflection coefficients in the frequency domain, which shows that this dispersion model is in effect selecting higher and lower frequencies for the two portions of the electric field.

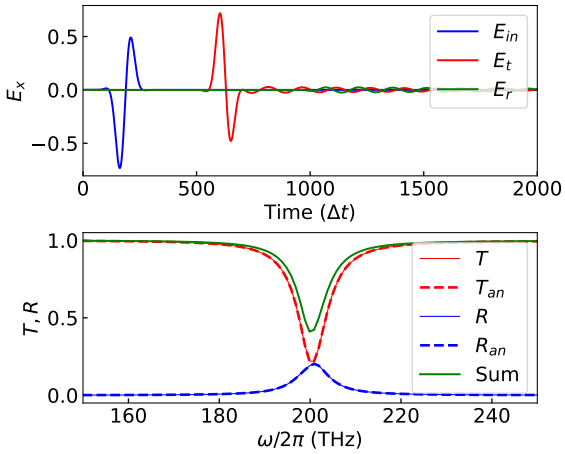

Figure 8. FDTD simulaiton of dielectric film of 200 nm with dielectric constant defined by the Lorentz dispersion model (Eq. (4)). We show the injected field (E_{in}), transmitted field (E_r), and the reflected field (E_r), as well as their corresponding transmission and reflection coefficients. The simulated and analytical solutions agree almost exactly.

We then implement the Lorentz dispersion model with the frequency-depenent dielectric constant give by,

$$\epsilon_L(\omega) = 1 - \frac{f_0\omega_0^2}{\omega_0^2 - \omega^2 + i2\omega\alpha} \tag{4}$$

where $\alpha = 4\pi \cdot 1 \times 10^{12}$ rad/s, $\omega_0 = 2\pi \cdot 200 \times 10^{12}$ rad/s, and $f_0 = 0.05$. The results of simulating this model is shown in Figs. 8 - 9. It can be seen that we enter a lossy medium regime with this dispersion model as well. This model also shows that the transmission coefficient is dominant in almost all frequencies with a significant dip near ω_0.

III. 2-DIMENSIONAL AND OPTIMIZATION

Now we generalize the algorithm to 2-dimensions and solve Maxwell's equations over a square region. We simulate a region of free space as well as a region with a dielectric slab placed slightly off centre. The results of these simulations after 1801 time steps are shown in Fig. 10 (free space) and Fig. 10 (dielectric slab with $\epsilon = 9$. No special boundary conditions were implemented so we can begin to see a couple nodes forming. These nodes are highly dependent on the composition of the region. In Fig. 10, we can see a symmetry of the contour diagram with a node in the center of the square, which is to be expected. However, when we introduce the "impurity" in the form of the off-centre dielectric slab, we lose this symmetry and see a different pattern. We can can see a node forming inside the dielectric slab, which is expected as it is the 2-dimensional manifestation of the trapped wave phenomenon we observed in the 1-dimensional case in Fig 4.

With this 2-dimensional FDTD implementation, we then optimized the algorithm because of the higher computational demand. We implemented loop-based and slicing approaches to update our different fields. Both of these functions could be optimized by Numba so this gave us four different algorithms we could test. Table I shows the

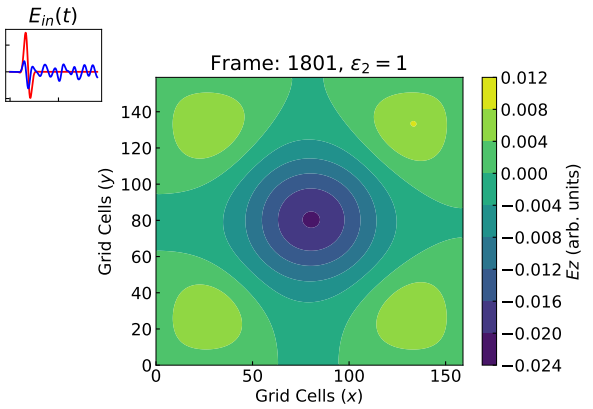

Figure 10. 2-dimensional FDTD simulation for a 160x160 cell with uniform dielectric constant of $\epsilon = 1$. A 1-fs dipole source is injected into the centre of the region.

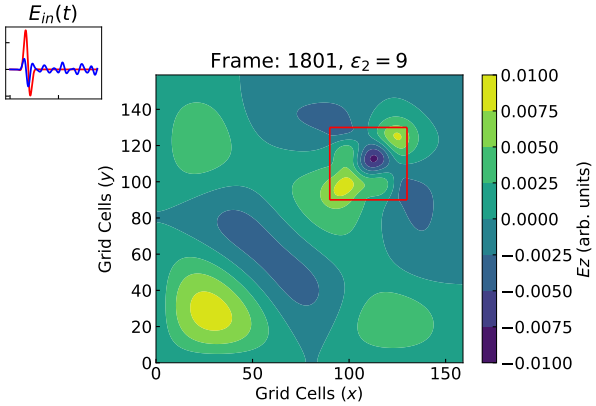

Figure 11. 2-dimensional FDTD simulation for a 160x160 cell with small slab of dielectric with constant of $\epsilon = 9$. A 1-fs dipole source is injected into the centre of the region.

execution time for each of these approaches on our local machine for 500-by-500 cell and 1000-by-1000 cell regions. Note that we used row-major iteration for the looping as it proved to be significantly faster given the way Python and C store the arrays in memory. It is clear that looping with Numba is the optimal approach to this problem. Interestingly, Numba and slicing was only slightly better than only slicing and much worse than Numba and looping.

Table I. Execution times for the different approaches to solving the 2-dimensional FDTD simulation on 500x500 and 1000x1000 cell grids. Each method was run for 1000 time steps except for the first approach that had no slicing or Numba as it takes a long time. We ran this approach for 100 time steps and multiplied the run time by 10. It is clear that Numba without slicing is the fastest method. Note that the non-slicing loops were executed by looping over the inner-dimension first.

Slicing	Numba	500 Cell Time (s)	1000 Cell Time (s)
No	No	1323.1	6809.5
Yes	No	28.0	69.1
No	Yes	5.1	11.8
Yes	Yes	19.2	45.8

Armed with an optimal algorithm, we then parallelized it using MPI. This was done by storing a buffer row on the top and bottom of the electric field and magnetic field slices. Only one buffer row is technically needed but this made implementation simplistic and even over the various processes at the cost of a negligible overhead memory cost. The times for the parallelized algorithm are given in Tab. II.

Table II. Execution times for parallelized FDTD implementation. We ran the experiment for 1000 time steps for square regions of 1000 and 3000 cell side lengths. Execution times are averaged over three different trials.

Tasks	1000 Cell Time (s)	3000 Cell Time (s)
1	5.19	68.02
2	2.30	33.62
4	1.55	18.45
8	1.34	9.91
16	1.06	7.86